Hydration structures near finite-sized nanoscopic objects reconstructed using inelastic x-ray scattering measurements

2009 J. Phys.: Condens. Matter 21 424115

(http://iopscience.iop.org/0953-8984/21/42/424115)

IOP Publishing Journal of Physics: Condensed Matter

J. Phys.: Condens. Matter **21** (2009) 424115 (9pp) doi:10.1088/0953-8984/21/42/424115

Hydration structures near finite-sized nanoscopic objects reconstructed using inelastic x-ray scattering measurements

Robert H Coridan[1], **Nathan W Schmidt**[1], **Ghee Hwee Lai**[1] and **Gerard C L Wong**[1,2,3]

[1] Department of Physics, University of Illinois at Urbana-Champaign, IL 61801, USA
[2] Frederick Seitz Materials Research Laboratory, University of Illinois at Urbana-Champaign, IL 61801, USA
[3] Department of Materials Science and Engineering, University of Illinois at Urbana-Champaign, IL 61801, USA

E-mail: gclwong@illinois.edu

Received 22 April 2009, in final form 13 August 2009
Published 29 September 2009
Online at stacks.iop.org/JPhysCM/21/424115

Abstract

Recent work has shown that it is possible to use high resolution dynamical structure factor $S(q, \omega)$ data measured with inelastic x-ray scattering to reconstruct the Green's function of water, which describes its dynamical density response to a point charge. Here, we generalize this approach and describe a strategy for reconstructing hydration behavior near simple charge distributions with excluded volumes, with the long term goal of engaging hydration processes in complex molecular systems. We use this Green's function based imaging of dynamics method to generate hydration structures and show that they are consistent with those of well-studied model systems.

(Some figures in this article are in colour only in the electronic version)

1. Introduction

Water-mediated interactions are important for a broad range of biological and colloidal processes [1–5]. Organization and dynamics of water molecules near solutes govern these interactions and affect rates and mechanisms of aqueous phase chemical reactions. A fundamental understanding of these phenomena requires knowledge of water structure and dynamics in bulk and in inhomogeneous systems (i.e., near solutes) at molecular lengthscales and molecular timescales.

High spatial resolution experimental techniques, such as x-ray absorption spectroscopy [6, 7] as well as x-ray [8] and neutron scattering [9, 10] have elucidated water structure at the level of pair correlation functions in bulk water. Those data, when supplemented with or interpreted in the context of classical molecular simulations [11, 12] provides additional insights into higher order water structure including triplet correlations and tetrahedrality. X-ray absorption fine structure spectroscopy and neutron diffraction has also been extended to study water structure in the hydration shell of hydrophobic solutes, such as krypton and methanol [13, 14]. In a complementary approach, dynamics of water molecules have been studied using ultrafast spectroscopy: infrared (IR) spectroscopy has been used to study the THz-frequency inter- and intra-molecular motions in liquid water [15, 16]. IR 'pump–probe' and vibrational-echo correlation spectroscopy experiments [17–21] have investigated energy-redistribution and vibrational excitation lifetimes of the intermolecular hydrogen bonds in water with femtosecond resolution. Computer simulations of classical n-point charge models of water ($n = 3, 4, 5$), and more recently, quantum models have played an important role in connecting these viewpoints. However, such simulations can be complex, computationally intensive, and specific details of results can depend on the precise choice of water model used in the study [22].

Inelastic x-ray scattering (IXS) is a hybrid technique that combines scattering and spectroscopy. IXS measures the dynamic structure factor $S(q, \omega)$ of condensed systems, and has been previously employed to investigate collective

dynamics in liquid water [23, 24], ice [25], glasses [26], as well as the hydration and ionic environments surrounding different biopolymers [27–29]. Abbamonte *et al* showed that it is possible to extract the Green's function from measured $S(q, \omega)$ and use it to image electron dynamics in a number of condensed matter systems [30, 31]. Recently, we reconstructed the femtosecond dynamics of water at molecular lengthscales from the Green's function extracted from a library of milli-electronvolt (meV) resolution $S(q, \omega)$ data [32]. This high resolution dataset, measured over a data range coextensive with the present limits of 3rd generation synchrotron x-ray sources, enables this Green's function imaging of dynamics (GFID) approach to track the average oxygen density correlations in water at ∼26 fs temporal resolution and at ∼0.44 Å spatial resolution. The extracted Green's function, also known as the density–density response function $\chi(q, \omega)$, gives a direct measure of water response to an ideal point charge. The results compare well to extant diffraction experiments, classical molecular dynamics, and femtosecond spectroscopic measurements [32]. If these results on point charges can be generalized to molecular systems with complex charge distributions and finite-sized excluded volumes, GFID can be a powerful technique that can engage solvation phenomena that are otherwise difficult to access experimentally.

In this paper, we show how the technique of reconstructing dynamics from the Green's function extracted from inelastic x-ray scattering data, can be generalized from pure electronic systems to molecular systems in order to provide a new data-based perspective to solvation processes. In order to access femtosecond timescales typical of molecular systems, a number of developments must be made. The energy resolution needs to be in the milli-electronvolt range, which is 2–3 orders of magnitude higher than the original demonstration experiment and subsequent experiments on purely electronic systems. This resolution is possible at third generation synchrotron x-ray sources with dedicated IXS beamlines. At these femtosecond timescales, electron dynamics are coupled to the phonon modes of the underlying molecular density fluctuations [33]. We begin by describing how Kramers–Kronig relations can be used to solve the phase problem for IXS measurements and how to use the extracted Green's function, also known as the density–density response function, to image the dynamic hydration structure around an idealized point charge. Although linear response theory can in principle be used in to extend this to more complex charge distributions, we show that a direct application of linear response theory fails to accurately describe the hydration environment around physical, finite-sized molecular solutes. This is due to excluded volume effects, which are not in the original conception of $S(q, \omega)$ inversion, but are present in all atomic and molecular systems. Finally, we describe a generalized implementation of solute excluded volume. Using a combination of linear response and excluded volume, we use GFID to generate hydration structures and show that they are consistent with those of well-studied molecular systems. This provides us with a basis to reconstruct hydration dynamics around molecular systems using the full Green's function.

2. Green's function imaging of dynamics

$S(\mathbf{q}, \omega)$ is a direct measurement of correlations between density fluctuations in a medium [34]. The fluctuation-dissipation theorem relates $S(\mathbf{q}, \omega)$ to the imaginary part of the linear response function $\chi(\mathbf{q}, \omega)$ that describes the dynamical propagation of density through the medium in response to an external perturbation, through

$$\chi''(\mathbf{q}, \omega) = -\pi[S(\mathbf{q}, \omega) - S(\mathbf{q}, -\omega)] \tag{1}$$

where $\chi(\mathbf{q}, \omega) = \chi'(\mathbf{q}, \omega) + \imath\chi''(\mathbf{q}, \omega)$. Since the measured $S(\mathbf{q}, \omega)$ can be weak, we use the detailed balance relationship, $S(\mathbf{q}, -\omega) = \mathrm{e}^{-\beta\omega} S(\mathbf{q}, \omega)$ [34] to relate χ'' to S. After correcting for finite resolution[4], each measured spectrum was divided by the Bose factor $n(\omega) = (1 - \mathrm{e}^{-\hbar\omega/kT})^{-1}$ to yield $\chi''(\mathbf{q}, \omega)$. For an isotropic system like liquid water, χ and S are both functions of only the magnitude of the vector q.

The real-space function $\chi(r, t)$, the Fourier transform of $\chi(q, \omega)$, is the Green's function (or density–density response function) that describes the dynamical propagation of density disturbances through the medium due to a delta-function perturbation at the origin. However, extracting $\chi(r, t)$ from a measurement is not a direct inversion because only the imaginary part is measured. The missing real part of the function $\chi(q, \omega)$ can be calculated from a measurement of $\chi''(q, \omega)$ by using Kramers–Kronig (KK) relations [34, 35, 30], which exploit the causal nature of the response to an external perturbation. For a general causal response function, the real part is related to the imaginary part by:

$$\chi'(q, \omega) = -\frac{1}{\pi}\int_{-\infty}^{\infty} \chi''(q, \omega') P\left[\frac{1}{\omega - \omega'}\right] \mathrm{d}\omega', \tag{2}$$

where P represents the principal part of the contour integral. One can then Fourier transform the fully known $\chi(q, \omega)$ to the real-space density–density response function $\chi(r, t)$:

$$\chi(r, t) = \int_0^{\infty} \mathrm{d}q q^2 \frac{\sin(qr)}{4\pi^2 qr} \int_{-\infty}^{\infty} \frac{\mathrm{d}\omega}{2\pi}[\chi'(q, \omega)\cos(\omega t) + \chi''(q, \omega)\sin(\omega t)]. \tag{3}$$

Since experimental data are discrete and finite, a number of modifications to the above procedure are necessary to avoid artifacts in the reconstructions. KK transformations involve continuous integrals, whereas measured data is discrete. Linear interpolation is used to approximate data continuously. Also,

[4] $S(q, \omega)$ has a sharp quasi-elastic peak (width < 1 meV) centered at $\omega = 0$. For a measurement of $S(q, \omega)$, this feature is resolution-broadened and resolution tails can potentially lead to density artifacts. The Lorentzian term of the DHO fit function centered at $\omega = 0$ was subtracted from each measured spectrum to minimize these artifacts. Although there is dynamical information in the quasi-elastic peak, the subtracted Lorentzian term is symmetric and does not contribute to $\chi(q, \omega)$, which is antisymmetric by definition (equation (1)). Moreover, because the quasi-elastic line is so narrow, it has a vanishing contribution to $\chi(q, \omega)$. As an additional check, this has been confirmed by explicitly evaluating equation (1) on data that have limited energy measurements on a symmetric domain (−20–20 meV). Extrapolation in q was done after the time transform, and the line shape of $\chi(q, t)$ was fit to a series of Gaussian peaks to capture the measured profile while enforcing the condition that $\chi(q) \to 0$ smoothly for large q.

both KK relations and Fourier transforms require that the argument functions be defined on an infinite domain. The IXS data at the endpoints of our measurements in q and in ω are essentially featureless and at background count levels, showing only statistical fluctuations. We extrapolated this data to zero at infinity using an optimized damped-harmonic oscillator (DHO) model function, a generally accepted lineshape for fitting the IXS spectra of liquids [23, 24, 27, 29], in order to evaluate the appropriate transformation without introducing artifacts. The best-fit DHO model parameters for the measured data was consistent with those reported in other IXS experiments on water for the same q-values [23, 36, 37]. Although it is possible to perform the extrapolation in different ways, the extrapolated data corresponds to times before our first time step at 26 fs in the reconstructions, and does not impinge on times in the regime of interest.

The resolution limits on the inversion are related to the maximal energy and momentum transfers measured, and the spatio-temporal range over which phenomena may be observed with GFID is determined by the measurement resolution. The sampling density in energy of the measurement is much smaller than the energy resolution of the instrument ($\Delta E = 1.7$ meV), and limits the maximum time window to $2\pi/\Delta E = 2.8$ ps. In reciprocal space, the q-resolution of the instrument ($\Delta q = 0.03$ Å^{-1}) is finer than the spacing between measurement points ($\sim$0.15 Å^{-1}), defined by the sampling density. Given the instrumental q-resolution, the maximum object size that can be engaged by the technique is $2\pi/0.03$ Å^{-1} $= 205$ Å. We calculate the baseline spatio-temporal resolution via the Nyquist condition based on the highest ω and q measured [31], yielding $\Delta t = \pi/80$ meV $=$ 26 fs and $\Delta r = \pi/7.2$ Å^{-1} $= 0.52$ Å. These limits are coincident with the present limits in inelastic x-ray scattering beamlines at 3rd generation synchrotron sources. It is possible, in the future, to use better instrumentation to improve the maximum energy transfer and thereby improve the temporal resolution. However, our measurements [32] show that at energy transfers of 80 meV and higher, the resulting spectra is only instrumental background. One possible reason for this is the nature of water motions itself. Molecular motions on these faster timescales (10s of femtoseconds) are known to be inertial rotations about the center-of-mass of the water molecule [38, 22]. Although x-ray scattering probes can accurately track the motion of the oxygens in water, they are not expected to be very sensitive to rotations of the water molecule about its oxygen-dominated center-of-mass. This suggests that in the future, an implementation of GFID that combines x-ray and neutron scattering can be a powerful way of making atomically resolved femtosecond movies of water.

The real-space density–density propagator $\chi(r, t)$ recovered from IXS measurements represents the response of water to a delta-function perturbation in space and in time at the origin. For x-rays, the perturbation is an electric field impulse. At the meV-energy scale, the inelastic scattering is due to atomic density fluctuations rather than ionized electrons. The lack of an isotopic shift in the excitation spectrum for D_2O relative to H_2O [23, 41] shows that the dynamical structure factor measured by meV-IXS is dominated by motion of the center-of-mass of the entire water molecule [37]. $S(q, \omega)$ is a measure of charge-density fluctuations in the bulk system [34]. Similarly, $\chi(q, \omega)$ is related to the inverse of the dielectric function $\epsilon(q, \omega)$,

$$\frac{1}{\epsilon(q,\omega)} - 1 = \frac{4\pi e^2}{q^2}\chi(q,\omega) = \mathcal{L}(q,\omega). \tag{4}$$

The quantity $\mathcal{L}$ is also known as the dielectric loss function. In the limit of linear response, the density response function is a Green's function that can be used to image the dynamical hydration structure around a defined external charge density. In Fourier space, the linear response relation between the induced charge density $\delta n_{\text{ind}}(\mathbf{q}, \omega)$ and the external charge density $\delta n_{\text{ext}}(\mathbf{q}, \omega)$ is

$$\delta n_{\text{ind}}(\mathbf{q},\omega) = \mathcal{L}(q,\omega)\delta n_{\text{ext}}(\mathbf{q},\omega). \tag{5}$$

Good reviews of the relationship between the density–density response function $\chi(q, \omega)$ and the dielectric function $\epsilon(q, \omega)$ can be found in the following [34, 42].

3. Linear response formalism with excluded volume

In principle, the induced charge density in a polarizable medium $\delta n_{\text{ind}}(\mathbf{q}, \omega)$ can be related to an external charge density $\delta n_{\text{ext}}(\mathbf{q}, \omega)$ by the linear response relation, equation (5). While this is useful for point charge descriptions of external charge distributions, it becomes problematic in the case of physical, finite-sized charge densities representing physical solutes such as ions and molecules. This problem can be seen more clearly by 'smearing' a point charge into a Gaussian charge distribution of increasing diameter (figure 2). As the diameter of the charge distribution is increased, the resultant hydration structure from a direct application of linear response is affected in two ways. (1) The hydration structure shifts radially outward. This can for example be seen in position of the first hydration shell. (2) The hydration structure itself weakens, via a decrease in peak height. It can be seen that when the diameter of the charge distribution approaches 3 Å, the hydration structure disappears almost entirely.

Without excluded volume effects, the disruption of hydration structure for extended charge distributions can be understood as a 'destructive interference' phenomenon. The induced charge density is related to the convolution of the real-space density response function $\chi(r, t)$ and the external charge distribution $\delta n_{\text{ext}}(\mathbf{r}, t)$. As the external charge distribution broadens, contributions to the induced charge density from different parts of $\delta n_{\text{ext}}(\mathbf{r}, t)$ begin to cancel one another because $\chi(r, t)$ describes both induced positive and negative density. Physically, the external charge density becomes too large for water molecules to organize hydration shells around it, and the granularity described by $\chi(r, t)$ becomes washed out. Equation (5) describes the external charge distribution is embedded into a continuous dielectric, which induces the bound charge density in response to the potential generated.

This formalism becomes unphysical for the situation of the solvation charge response due to a molecular solute in liquid water. Solutes are defined by their charge distribution and by an excluding volume that liquid water is forbidden

from penetrating. The physical basis for this is the Pauli exclusion principle, where overlapping electron wavefunctions are forbidden. An example of this is the excess electron in water, which relaxes to its ground state while opening up a cavity that has a diameter of more than 6 Å when defining the first hydration shell as the center-of-mass of the nearest water molecules. To use linear response in any meaningful way, the excluded volume of the solute charge distribution must be a factor in the hydration description.

A similar situation to the excluded volume problem occurs in quantum chemistry when the electronic structure and excitation energies of dissolved molecules are sought. Molecular simulations involving a large number of explicit solvent molecules rapidly become expensive as the size of the solute molecule increases. Implicit solvent models are used to describe the hydration environment efficiently. The aqueous environment is modeled as an infinite dielectric, sometimes with complicated dynamical or non-local behavior, but typically with a uniform dielectric constant matching that of bulk water ($\epsilon_{\text{water}} \approx 80$). The solute is modeled as a charge distribution and cavity chosen to reflect the solute's morphology. An example cavity is an assembly of spheres, one centered at each atomic center with the respective radii matching one that is empirically determined (the van der Waals radius, for example). The excluded volume is chosen arbitrarily, as long as there is a physical basis for it. For the case of GFID, combining the dielectric loss function formalism in equation (5) with this implementation of excluded volume is a good place to start for fully describing physical solutes.

We assume that the interior of the cavity is devoid of solvent, hence no polarizable media ($\epsilon = 1$). The surrounding solvent behaves like bulk solvent. A modified dielectric loss function can be defined accordingly:

$$\mathcal{L}^{\text{mod}}(|\mathbf{r}-\mathbf{r}'|;\omega) = \begin{cases} 0 & \mathbf{r} \text{ or } \mathbf{r}' \in V_{\text{exc}} \\ \mathcal{L}(|\mathbf{r}-\mathbf{r}'|;\omega) & \mathbf{r} \text{ and } \mathbf{r}' \notin V_{\text{exc}}, \end{cases} \tag{6}$$

where $\mathcal{L}$ is related to the measurable quantity χ in equation (4). This places boundary conditions on the dielectric function ϵ:

$$\epsilon^{\text{mod}}(|\mathbf{r}-\mathbf{r}'|;\omega) = \begin{cases} 1 & \mathbf{r} \text{ or } \mathbf{r}' \in V_{\text{exc}} \\ \epsilon(|\mathbf{r}-\mathbf{r}'|;\omega) & \mathbf{r} \text{ and } \mathbf{r}' \notin V_{\text{exc}}. \end{cases} \tag{7}$$

Inside of the solute's excluded volume, ϵ has the vacuum value of 1. For isotropic systems like liquid water, $\mathcal{L}$ is a function of the distance between the points $\mathbf{r}$ and $\mathbf{r}'$. In general, however, it is a two-point function: it propagates the effect of electrodynamical quantities at a point in space $\mathbf{r}'$ to a point $\mathbf{r}$. This is easily seen in the real-space equivalent of equation (5):

$$n_{\text{ind}}(\mathbf{r};\omega) = \int_{-\infty}^{\infty} \mathrm{d}\mathbf{r}' \mathcal{L}(\mathbf{r},\mathbf{r}';\omega) n_{\text{ext}}(\mathbf{r}';\omega). \tag{8}$$

However, this 'charge-in/charge-out' method of linear response is problematic when combined with $\mathcal{L}^{\text{mod}}$. Equation (5) propagates the effect of the charge density at the point $\mathbf{r}'$ to the position $\mathbf{r}$. The boundary conditions defined in equation (6) nullify any induced charge density if the external charge distribution is entirely contained within the excluded volume. $\mathcal{L}^{\text{mod}}$ is zero where n_{ext} is non-zero, making n_{ind} uniformly zero. As defined, the linear response relation equation (5) and the modified dielectric loss function $\mathcal{L}^{\text{mod}}$ are incompatible because the localized external charge densities do not contribute to charge induction in the media. An approach that accounts for the influence of the external charge distribution over all space is needed.

Previous work on solute–solvent interactions suggest an alternate approach to move forward [43–46]. The electric displacement $\vec{D}(\mathbf{r})$ is a property of the localized external charge distribution that spans all space. Unlike the electric field, the electric displacement is independent of its dielectric environment. $\vec{D}(\mathbf{r})$ from solute induces a polarization at all points in the solvent:

$$P_\alpha(\mathbf{q},\omega) = -(\epsilon^{-1}_{\alpha\beta}(\mathbf{q},\omega)-1)D_\beta(\mathbf{q},\omega) = -\mathcal{L}(\mathbf{q},\omega)D_\beta(\mathbf{q},\omega) \tag{9}$$

where $\epsilon^{-1}_{\alpha\beta}$ is the inverse dielectric tensor. $\epsilon^{-1}_{\alpha\beta}$ and $\mathcal{L}_{\alpha\beta}$ are the tensor versions of ϵ^{-1} and $\mathcal{L}$ found in equation (4) [34]. $\mathcal{L}_{\alpha\beta}$ can be written explicitly in terms of its longitudinal ($\mathcal{L}(q,\omega)$) and transverse ($\mathcal{L}_\perp(q,\omega)$) components [40]:

$$\mathcal{L}_{\alpha\beta}(\vec{\mathbf{q}},\omega) = \mathcal{L}(q,\omega)\frac{q_\alpha q_\beta}{q^2} + \mathcal{L}_\perp(q,\omega)\left(\delta_{\alpha\beta} - \frac{q_\alpha q_\beta}{q^2}\right). \tag{10}$$

The longitudinal component $\mathcal{L}(q,\omega)$ is the quantity measurable by inelastic scattering experiments. The transverse component $\mathcal{L}_\perp(q,\omega)$ contributes in magnetic systems and those in which total charge reorganization occurs more rapidly (due to rotational molecular motions, for example) than the longitudinal reorganization alone [40]. The characteristic timescale for oxygen oscillation in water is ~200 fs [21, 32], so we are primarily interested in phenomena in water that occur from ~100 fs onwards. By comparison, the inertial reorganization of water molecules occurs on the order of ~10s of femtoseconds. The transverse component can be ignored and the dynamical polarization induced in the solvent surrounding a solute molecule can be calculated from the dynamical electric displacement $\vec{D}(\mathbf{q},\omega)$ and the Fourier transform of the modified dielectric loss tensor, $\mathcal{L}^{\text{mod}}_{\alpha\beta}(\mathbf{q},\omega)$ (with an implicit sum over β),

$$P_\alpha(\mathbf{q},\omega) = \mathcal{L}^{\text{mod}}_{\alpha\beta}(\mathbf{q},\omega)\mathbf{D}_\beta(\mathbf{q},\omega). \tag{11}$$

While the relationship between the electric displacement and the induced polarization is defined in Fourier space for simplicity, it is most useful to ultimately calculate these quantities in real space. Equation (11) is a convolution in real space:

$$P_\alpha(\mathbf{r},t) = \int_{-\infty}^{t} \mathrm{d}t' \int_{-\infty}^{\infty} \mathrm{d}\mathbf{r}' \mathcal{L}^{\text{mod}}_{\alpha\beta}(|\mathbf{r}-\mathbf{r}'|;t-t')D_\beta(\mathbf{r}';t'), \tag{12}$$

where $\mathcal{L}^{\text{mod}}_{\alpha\beta}(|\mathbf{r}-\mathbf{r}'|;t-t')$ is the Fourier transform of the tensor $\mathcal{L}^{\text{mod}}_{\alpha\beta}(\mathbf{q},\omega)$ which incorporates the modified density response function (equation (6)) into the polarization calculation. The goal of this calculation is to image the hydration structure surrounding a defined dynamical molecular solute, as indicated by the oxygen positions, via the induced charge density. The induced charge density in the solvent can be computed directly from the real-space polarization,

$$n_{\text{ind}}(\mathbf{r},t) = -\vec{\nabla}\cdot\vec{P}(\mathbf{r},t). \tag{13}$$

From the boundary conditions defined in equation (6), $P_\alpha(\mathbf{r}, t)$ is uniformly zero for $\mathbf{r} \in V_{\text{exc}}$. There is no solvent inside the cavity to mediate an induced charge. For $\mathbf{r} \notin V_{\text{exc}}$, $P_\alpha(\mathbf{r}, t)$ depends on the displacement field over all space *except* from the cavity. Equation (12) can be expressed in terms of the boundary-free induced polarization $P^0_\alpha(\mathbf{r}; t)$ and a boundary enforcing correction $\delta P_\alpha(\mathbf{r}; t)$:

$$P^0_\alpha(\mathbf{r}; t) = \begin{cases} 0 & \mathbf{r} \in V_{\text{exc}} \\ P^0_\alpha(\mathbf{r}; t) - \delta P_\alpha(\mathbf{r}; t) & \mathbf{r} \notin V_{\text{exc}}, \end{cases} \tag{14}$$

where

$$P^0_\alpha(\mathbf{r}; t) = \int_{-\infty}^{t} \mathrm{d}t' \int_{-\infty}^{\infty} \mathrm{d}\mathbf{r}' \mathcal{L}_{\alpha\beta}(|\mathbf{r} - \mathbf{r}'|; t - t') D_\beta(\mathbf{r}'; t'), \tag{15}$$

and

$$\delta P_\alpha(\mathbf{r}; t) = \int_{-\infty}^{t} \mathrm{d}t' \int_{V_{\text{exc}}} \mathrm{d}\mathbf{r}' \mathcal{L}_{\alpha\beta}(|\mathbf{r} - \mathbf{r}'|; t - t') D_\beta(\mathbf{r}'; t'). \tag{16}$$

$\delta \vec{P}(\mathbf{r}; t)$ is essentially a linear correction to the boundary-free case. It removes the non-local contribution to the induced polarization from the cavity V_{exc} at all points. The special case for $\mathbf{r} \in V_{\text{exc}}$ accounts for the lack of polarizable solvent inside the cavity. Equation (14) is equivalent to approach defined by equation (12).

It is important to note that this general approach for describing the excluded volume is not new. It has been used to describe model solute–solvent systems in the approximation of the solvent behaving as a continuous dielectric [43–46]. It has been shown that this approximation underestimates the long-time relaxation that is better captured in more accurate treatments, like Gaussian field models of solvation, where an inverse tensor of the dielectric loss function is used rather than a simple subtraction of the cavity contribution [47]. The tensor inversion approach, which can be implemented within GFID, becomes computationally expensive when imaging dynamical solvation structures due to added step of inverting the two-point susceptibility tensor over all points in space at each time step. By comparison, equations (14)–(16) can be calculated using fast Fourier transforms at each time step and are computationally efficient. Further, the dynamics captured by our measured response function agree well with other measurements within the described resolution limitations [32]. A comparison between the Gaussian solvation model and the cavity subtraction approach can in principle be quantified with our data. However, the timescales over which a difference is observed [47] is larger than the longitudinal relaxation lifetime of water (∼0.7 ps) [17]. In the present dataset, the extracted response function has largely decayed to noise over this timescale, so this difference is likely comparable to other sources of noise in the measurement.

4. Examples

Using the method described in section 3, the hydration structure around an external charge density with explicit excluded volume can be determined. In the following static examples, the density response function $\chi(q)$ used is shown in figure 1(b). A discussion of the experimental considerations for measuring $\chi(q)$ can be found elsewhere [32]. It should be noted that, while the examples discussed here are relevant to systems of hydrated ions, the implementation of excluded volume described in section 3 can be extended to larger objects and to different geometries.

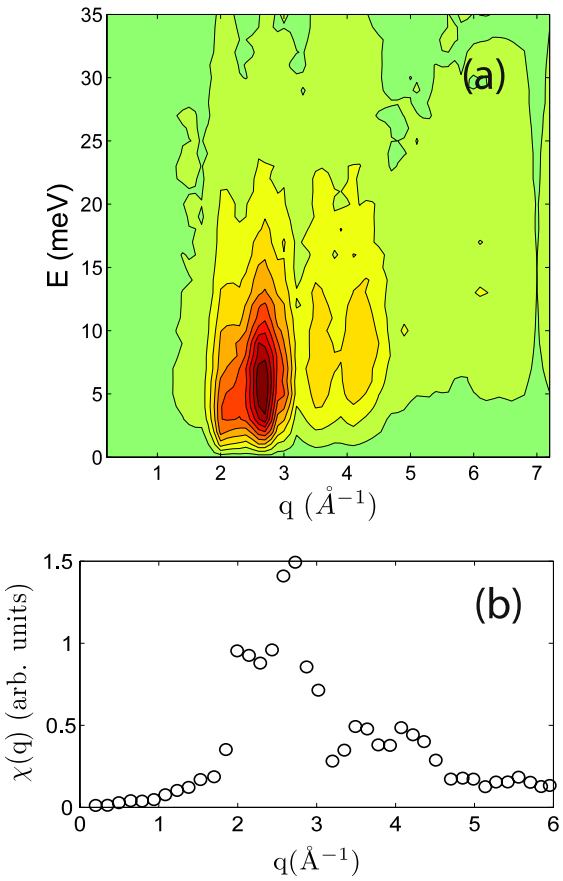

Figure 1. (a) The measured function $\chi''(q, \omega)$. $S(q, \omega)$ measurements on room-temperature liquid water were made at ESRF (Grenoble, France) over a q-range of 0.2–7.2 Å^{-1}. The detailed balance condition that relates $S(q, \omega)$ to $\chi''(q, \omega)$ was applied to construct this dataset. See section 2 for complete procedure. This dataset is comprised of over 9000 individual measurements in the (q, ω) plane. (b) A $\omega = 0$ slice of the measured response function $\chi(q, \omega)$, where ω is scanned for each q-point. This measurement of $\chi(q, \omega = 0)$ is consistent with neutron scattering measurements and simulations [39, 40].

The simplest model of a classical ion is a charge distribution coincident with a spherical excluded volume. Much of the difference between ionic species of the same charge comes from the differences in volume from which solvent water molecules are prohibited. In fact, in many classical molecular dynamics models of water, simulated ions are implemented as a charge contained in a Lennard-Jones sphere with a diameter that varies by species. Using GFID and excluded volume, the effect of the charge distribution and exclusion diameter can be independently quantified and compared to other measurements.

We first investigate the induced charge density in the surrounding medium as a function of the radius of the excluded

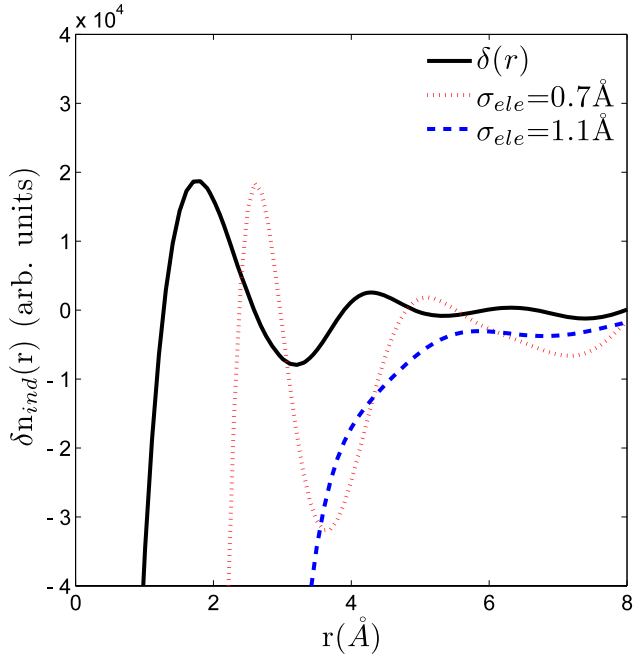

Figure 2. The induced charge density around a point charge (——) and around Gaussian charge distributions of increasing widths $\sigma_{ele} = 0.7$ Å (· · · · · ·) and $\sigma_{ele} = 1.1$ Å (- - - -). As the charge distribution increases its width, the hydration structure moves out radially and weakens.

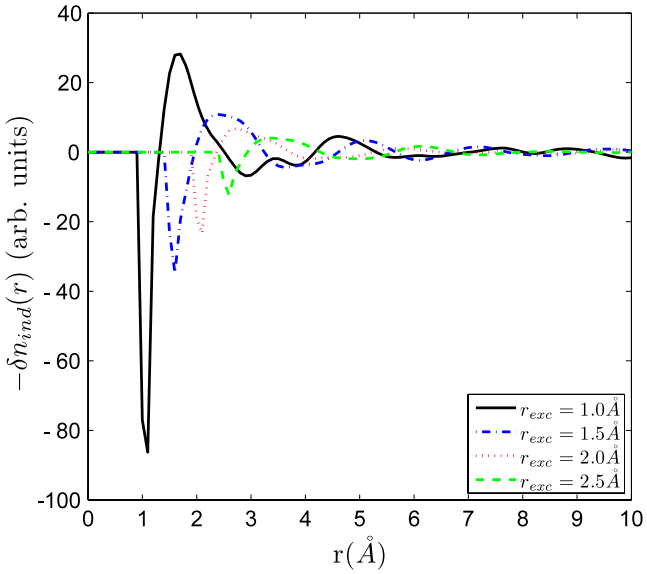

Figure 3. For a fixed external charge distribution (a Gaussian with width $\sigma_Q = 0.3$ Å), the excluded volume radius r_{exc} is varied from 1.0 to 2.5 Å. The induced charge density $\delta n_{ind}(r)$ is plotted as a function of the distance from the center of the external charge distribution. The position of the first minimum (negative induced charge density) represents the first hydration shell position of oxygen, as it carries the negative charge density in water. This peak position can be continuously controlled by the parameter r_{exc}.

volume (figure 3). The position of the induced negative charge density represents the average oxygen position of water. In this case, the excluded volume is a sphere of radius

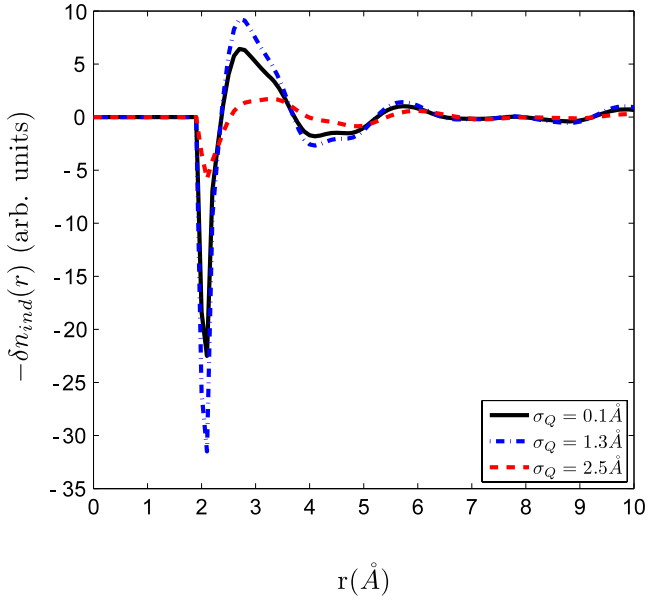

Figure 4. The effect of the diameter of the charge for a fixed excluded volume ($r_{exc} = 2$ Å). The external charge distributions are modeled as Gaussians centered at the origin with widths of $\sigma_Q = 0.1$ Å (induced charge density shown as a solid line), $\sigma_Q = 1.3$ Å (dash–dot line), and $\sigma_Q = 2.5$ Å (dotted line). When the charge is mostly contained within the excluded volume, the induced charge density is nearly conserved ($\sigma_Q = 0.1$, 1.3 Å). For larger distributions ($\sigma_Q = 2.5$ Å), where significant fractions of charge penetrate the surrounding medium, the induced charge density is weakened. Additionally, the induced features are slightly broadened compared to the narrower charge distributions.

r_{exc}. It can be seen that the position of the first hydration shell can be parameterized by the choice of r_{exc} to match physically determined values for ionic species. The effect of spatial distribution of charge can amount of charge can be independently controlled for fixed excluded volume. Figure 4 shows that, for a fixed cavity radius ($r_{exc} = 2$ Å), the magnitude and the shape of the induced charge density is affected by the spatial distribution of charge. In both cases, the induced negative charge density, which tracks with the average oxygen density, around the excluded volume decreases in magnitude as the external charge distribution leaks into the medium: for a particular position $\vec{r}$, less charge is contained with in the sphere of radius $|\vec{r}|$. As a result of Gauss's law, the displacement vector $\vec{D}(\mathbf{r})$ and the induced polarization $\vec{P}(\mathbf{r})$ are weakened.

Using these two parameters, a library of hydration structures can be generated. We examine the values of parameters that replicate known physical hydration structures around ions. Anions like Cl^- and F^- have well quantified first-coordination shell ion–oxygen positions of ∼3.1 Å [48] and ∼2.7 Å [49, 50], respectively. The electron density for each ion is calculated using the well benchmarked quantum chemistry package GAMESS, with the nucleus included as a sharp peak at the origin. GAMESS uses density-functional theory to calculate the electronic structures of quantum mechanical ions and molecules [51]. Using these calculated charge distributions, we find good agreement in the first peak position of negative induced charge density and the known ion–oxygen

distance when r_{exc} is ∼2.25 Å for Cl^- and ∼1.75 Å for F^-. These values for r_{exc} are slightly larger than the bare ion radii (1.81 Å for Cl^-, 1.36 Å for F^- [52]). These small deviations are not surprising due to water packing, structure and hydrogen-bonding effects.

Another well-studied fundamental charge distribution in water is the solvated excess electron, which is defined both by a cavity and by a significant amount of charge penetrating the surrounding environment, in contrast to atomic ions. The excess electron in water is a ubiquitous transient species in photoinduced chemical reactions. It forms a roughly spherical charge distribution and an ion-like cavity surrounded by water molecules. Though the hydrated electron has been studied for decades using simulations [53–55], little experimental work has been published on the bulk-hydrated electron case. Experimental access is limited to the excess electron on water clusters due to the complicated nature of the bulk case. Here we use GFID to construct a schematic model of the hydrated electron surrounded by bulk-phase water, and compare this model to what is known about the hydrated electron.

Computer simulations model the hydrated electron as a rapidly moving 'point charge' that interacts with its surrounding environment quantum mechanically. Here, we investigate the extent to which this can be captured using an average 'smeared' negative charge distribution of finite spatial extent coincident with a spherical solvent cavity of well-defined size. From measurements [56] and simulations [53], the hydrated electron is known to be centered in a cavity with the first hydration shell center-oxygen distance being 3.1–3.3 Å and center-hydrogen distance being 2.1 Å. The analogous glassy structure of tetrahedrally coordinated water molecules surrounding the hydrated electron is known as the Kevan model [56]. Further, it is known that the electron 'leaks' out of its cavity: about 20% of the electron penetrates the surrounding solvent [57]. Using these observations, we model the hydrated electron roughly as a negative Gaussian charge distribution, $\rho(\mathbf{r}) \propto e^{-\mathbf{r}^2/2\sigma^2}$, where $\sigma = 1.5$ Å. The cavity is defined to replicate the known charge spillage, by using a sphere that encloses 80% of the Gaussian charge distribution. This results in an excluded volume that extends ∼2 Å from the center of the distribution.

Using these as inputs, we compared the resultant induced hydration structure from GFID with computer simulations. The model and static GFID/excluded volume reconstructions of the long-time hydration structure surrounding the model of the static electron model agree well with both simulations and experiment. The induced negative charge density is centered at 3.2 Å, in agreement with simulation and Kevan model results.

5. Discussion

As shown in the examples from section 4, it is possible to reconstruct the hydration structure surrounding model charge distributions with excluded volume from meV-IXS data. In addition to getting physically accurate results, it is important to address the range of validity of this technique. For example, what are the physical limitations on the range of systems that can be studied using this technique? Linear response theory is believed to hold for most cases of physical solute–solvent systems. However, it has been recently demonstrated that linear response can fail for cases involving chemical reactions and photoexcitation in various solvents [58]. A direct comparison between linear response in optical spectroscopies and in GFID is complicated by inherent differences in the underlying measured quantities. We examine two situations.

For femtosecond dynamical processes, the assumption of linear response (LR) is that for small perturbations like changes in solute charge density, the solvent relaxes through the same modes that govern fluctuations of the interaction at equilibrium. Recently experiments and computational studies have become sophisticated enough to test the limits of LR, and several examples of LR breakdown have been demonstrated, where symmetric changes in the parameters of an experiment result in qualitatively different relaxation responses from the system. An example of this is the solvent dynamics around a positive ion. In LR, exchanging a negative ion of identical valence for the positive ion should result in a solvent response identical in magnitude while opposite in sign. LR breaks down when this assumption does not hold. Recent demonstrations of LR breakdown are exemplified by the following two classes of phenomena. The first is that upon excitation, the solute changes size, affecting the steric state as well as the energetics of hydration, rather than just the latter [58], hence driving a breakdown of LR. Similar systems show an asymmetric relaxation between the photoexcited cationic and anionic state of sodium [59]. The second class of phenomena is that the solute dynamics under study are so rapid that they break the LR assumption of continuous solute–solvent interaction. For example, the CN molecule can be thought of as a high-speed molecular rotor. It has been shown that CN can maintain its angular velocity for many periods after photoexcitation, rather than to continuously lose rotational energy to the environment as it would under LR [60].

These situations highlight the potential strengths of the GFID technique. Formally, GFID is based on LR. However, both the spatial and temporal parameters of the external charge distribution are inputs to the reconstruction. For example, in the case of an asymmetric solute size, the initial and final charge distribution, as well as the initial and final size and shape of the excluded molecular volume are all defined in the LR-based formalism, which mitigate against LR breakdown from changes in steric interactions due to changes in molecular shape. In future work, we will do a direct comparison between GFID and results from optical spectroscopy on these systems.

From the discussion in this paper, it is clear that GFID is limited by a number of factors. The GFID method can be used to reconstruct spatio-temporal water dynamics around dynamic charge distributions, particularly those governed by Gaussian statistics, valid at lengthscales smaller than those that nucleate a change in phase in the surrounding solvent [61–63]. In addition to the limitations implicit in the assumptions of the fluctuation-dissipation theorem, GFID is limited by the resolution considerations previously discussed.

6. Conclusion

In this paper, we have described a method to reconstruct hydration structure from inelastic x-ray scattering data. The protocol for inverting inelastic x-ray scattering spectra from meV-resolution experiments via Kramers–Kronig relations to recover the bulk density linear response function of liquid water is described in detail. We also suggest an implementation of GFID that takes into account excluded volume, and compare the results of this implementation to the known hydration structure of two different solute–solvent systems. Good agreement with accepted hydration structure results can be obtained using GFID. Future work includes applying the excluded volume implementation to the reconstruction of evolving hydration structures around dynamical charge distributions.

Acknowledgments

GW is supported by NSF Water CAMPWS and NSF RPI-UIUC NSEC (DMR-0117792, DMR-0642573). We thank P Abbamonte, N Baker, S Garde, D Chandler, B Schwartz, P Rossky, R Godawat, M Krisch, A Alatas, H Sinn, and J Serrano for insightful discussions and technical assistance.

References

[1] Dill K A 1990 *Biochemistry* **29** 7133–55
[2] Chandler D 2005 *Nature* **437** 640–7
[3] Luzar A and Chandler D 1996 *Nature* **379** 55–7
[4] Cheng Y K and Rossky P J 1998 *Nature* **392** 696–9
[5] Zichi D A and Rossky P J 1986 *J. Chem. Phys.* **84** 2814–22
[6] Wernet P, Nordlund D, Bergmann U, Cavalleri M, Odelius M, Ogasawara H, Naslund L A, Hirsch T K, Ojamae L, Glatzel P, Pettersson L G M and Nilsson A 2004 *Science* **304** 995–9
[7] Smith J D, Cappa C D, Wilson K R, Messer B M, Cohen R C and Saykally R J 2004 *Science* **306** 851–3
[8] Head-Gordon T and Hura G 2002 *Chem. Rev.* **102** 2651–70
[9] Narten A H and Levy H A 1971 *J. Chem. Phys.* **55** 2263–9
[10] Soper A K and Phillips M G 1986 *Chem. Phys.* **107** 47–60
[11] Head-Gordon T and Johnson M E 2006 *Proc. Natl Acad. Sci.* **103** 7973–7
[12] Soper A K 1997 *J. Phys.: Condens. Matter* **9** 2717–30
[13] Soper A K and Finney J L 1993 *Phys. Rev. Lett.* **71** 4346
[14] Filipponi A, Bowron D T, Lobban C and Finney J L 1997 *Phys. Rev. Lett.* **79** 1293
[15] Eisenberg D and Kauzmann W 1969 *The Structure and Properties of Water* (New York: Oxford University Press)
[16] Franks F 1972 *Water: A Comprehensive Treatise* (New York: Plenum)
[17] Woutersen S, Emmerichs U and Bakker H J 1997 *Science* **278** 658–60
[18] Woutersen S and Bakker H J 1999 *Nature* **402** 507–9
[19] Asbury J B, Steinel T, Kwak K, Corcelli S A, Lawrence C P, Skinner J L and Fayer M D 2004 *J. Chem. Phys.* **121** 12431–46
[20] Asbury J B, Steinel T, Stromberg C, Corcelli S A, Lawrence C P, Skinner J L and Fayer M D 2004 *J. Phys. Chem.* A **108** 1107–19
[21] Fecko C J, Eaves J D, Loparo J J, Tokmakoff A and Geissler P L 2003 *Science* **301** 1698–702
[22] Laage D and Hynes J T 2006 *Science* **311** 832–5
[23] Sette F, Ruocco G, Krisch M, Bergmann U, Masciovecchio C, Mazzacurati V, Signorelli G and Verbeni R 1995 *Phys. Rev. Lett.* **75** 850
[24] Sette F, Ruocco G, Krisch M, Masciovecchio C, Verbeni R and Bergmann U 1996 *Phys. Rev. Lett.* **77** 83
[25] Ruocco G, Sette F, Bergmann U, Krisch M, Masciovecchlo C, Mazzacurati V, Signorelli G and Verbeni R 1996 *Nature* **379** 521–3
[26] Masciovecchio C, Ruocco G, Sette F, Krisch M, Verbeni R, Bergmann U and Soltwisch M 1996 *Phys. Rev. Lett.* **76** 3356
[27] Chen S H, Liao C Y, Huang H W, Weiss T M, Bellissent-Funel M C and Sette F 2001 *Phys. Rev. Lett.* **86** 740
[28] Liu Y, Berti D, Baglioni P, Chen S H, Alatas A, Sinn H, Said A and Alp E 2005 *J. Phys. Chem. Solids* **66** 2235–45
[29] Angelini T E, Golestanian R, Coridan R H, Butler J C, Beraud A, Krisch M, Sinn H, Schweizer K S and Wong G C L 2006 *Proc. Natl Acad. Sci.* **103** 7962–7
[30] Abbamonte P, Finkelstein K D, Collins M D and Gruner S M 2004 *Phys. Rev. Lett.* **92** 237401
[31] Abbamonte P, Graber T, Reed J P, Smadici S, Yeh C L, Shukla A, Rueff J P and Ku W 2008 *Proc. Natl Acad. Sci. USA* **105** 12159–63
[32] Coridan R H, Lai G H, Schmidt N W, Godawat R, Krisch M, Garde S, Abbamonte P and Wong G C L 2009 *Phys. Rev. Lett.* submitted
[33] Sinha S K 2001 *J. Phys.: Condens. Matter* **13** 7511–23
[34] Pines D and Nozieres P 1966 *The Theory of Quantum Liquids* vol 1 (Reading, MA: Benjamin)
[35] Jackson J D 1999 *Classical Electrodynamics* 3rd edn (New York: Wiley)
[36] Sampoli M, Ruocco G and Sette F 1997 *Phys. Rev. Lett.* **79** 1678–81
[37] Ruocco G and Sette F 1999 *J. Phys.: Condens. Matter* **11** R259–93
[38] Jimenez R, Fleming G R, Kumar P V and Maroncelli M 1994 *Nature* **369** 471–3
[39] Bopp P A, Kornyshev A A and Sutmann G 1996 *Phys. Rev. Lett.* **76** 1280–3
[40] Bopp P A, Kornyshev A A and Sutmann G 1998 *J. Chem. Phys.* **109** 1939–58
[41] Teixeira J, Bellissent-Funel M C, Chen S H and Dorner B 1985 *Phys. Rev. Lett.* **54** 2681–3
[42] Schulke W 1991 *Inelastic Scattering by Electronic Excitations* vol 3 (Amsterdam: Elsevier)
[43] Kornyshev A A, Rubinshtein A I and Vorotyntsev M A 1978 *J. Phys. C: Solid State Phys.* **11** 3307–22
[44] Basilevsky M V and Parsons D F 1996 *J. Chem. Phys.* **105** 3734–46
[45] Roux B, Yu H A and Karplus M 1990 *J. Phys. Chem.* **94** 4683–8
[46] Bagchi B 1989 *Annu. Rev. Phys. Chem.* **40** 115–41
[47] Song X, Chandler D and Marcus R A 1996 *J. Phys. Chem.* **100** 11954
[48] Mancinelli R, Botti A, Bruni F, Ricci M A and Soper A K 2007 *J. Phys. Chem.* B **111** 13570–7
[49] Perera L and Berkowitz M L 1994 *J. Chem. Phys.* **100** 3085–93
[50] Ho M H, Klein M L and Kuo I F W 2009 *J. Phys. Chem.* A **113** 2070–4
[51] Schmidt M, Baldridge K, Boatz J, Elbert S, Gordon M, Jensen J, Koseki S, Matsunaga N, Nguyen K and Su S 1993 *J. Comput. Chem.* **14** 1347–63
[52] Nightingale E R 1959 *J. Phys. Chem.* **63** 1381–7
[53] Rossky P and Schnitker J 1988 *J. Phys. Chem.* **92** 4277–85
[54] Schwartz B J and Rossky P J 1994 *J. Chem. Phys.* **101** 6902–16
[55] Laria D, Wu D and Chandler D 1991 *J. Chem. Phys.* **95** 4444–53
[56] Kevan L 1981 *Acc. Chem. Res.* **14** 138–45
[57] Shkrob I A, Glover W J, Larsen R E and Schwartz B J 2007 *J. Phys. Chem.* A **111** 5232–43
[58] Bedard-Hearn M J, Larsen R E and Schwartz B J 2003 *J. Phys. Chem.* A **107** 4773–7

[59] Bragg A E, Cavanagh M C and Schwartz B J 2008 *Science* **321** 1817–22
[60] Moskun A C, Jailaubekov A E, Bradforth S E, Tao G and Stratt R M 2006 *Science* **311** 1907–11
[61] Pratt L R and Chandler D 1977 *J. Chem. Phys.* **67** 3683–704
[62] Hummer G, Garde S, Garcia A, Pohorille A and Pratt L 1996 *Proc. Natl Acad. Sci.* **93** 8951–5
[63] Crooks G E and Chandler D 1997 *Phys. Rev.* E **56** 4217